Visualization of G1 Chromosomes: A Folded, Twisted, Supercoiled Chromonema Model of Interphase Chromatid Structure

Andrew S. Belmont and Kathy Bruce

Department of Cell and Structural Biology, University of Illinois, Champaign-Urbana, Urbana, Illinois 61801

Abstract. We have used light microscopy and serial thin-section electron microscopy to visualize intermediates of chromosome decondensation during G1 progression in synchronized CHO cells. In early G1, tightly coiled 100–130-nm "chromonema" fibers are visualized within partially decondensed chromatin masses. Progression from early to middle G1 is accompanied by a progressive uncoiling and straightening of these chromonema fibers. Further decondensation in later G1 and early S phase results in predominantly 60–80-nm chromonema fibers that can be traced up to 2–3 μm in length as discrete fibers. Abrupt transitions in diameter from 100–130 to 60–80 nm along individual fibers are suggestive of coiling of the 60–80-nm chromonema fibers to form the thicker 100–130-nm chromonema fiber. Local unfolding of these chromonema fibers, corresponding to DNA regions tens to hundreds of kilobases in length, reveal more loosely folded and extended 30-nm chromatin fibers. Kinks and supercoils appear as prominent features at all observed levels of folding. These results are inconsistent with prevailing models of chromosome structure and, instead, suggest a folded chromonema model of chromosome structure.

EXPERIMENTAL analysis of diploid chromosome architecture has focused predominantly on mitotic rather than interphase chromosome structure. However, a serious limitation in studying mitotic chromosome structure is their tremendous packing density and folding complexity. As discussed previously (Belmont et al., 1987), most investigators have dealt with this complexity either by focusing on surface topology or by using procedures aimed at unfolding the chromosome. Depending on the experimental approach, different observed features have been emphasized leading to several different and mutually exclusive models of mitotic chromosome structure. These models include successive helical folding (Sedat and Manuelidis, 1977), radial loop (Paulson and Laemmli, 1977; Marsden and Laemmli, 1979; Adolph, 1980), or combined radial loop–helical folding (Rattner and Lin, 1985; Boy de la Tour and Laemmli, 1988) motifs as the basis of mitotic chromosome structure. In turn, most models of interphase chromosome structure are based on extrapolations from these mitotic chromosome models.

Direct verification or contradiction of these models would require three-dimensional reconstructions of native mitotic chromosomes with sufficient resolution to trace the folding of tightly packed, individual 10- or 30-nm chromatin fibers throughout large chromosomal regions. In fact, though, any workable model of mitotic or interphase chromosome structure must present a plausible pathway for chromosome condensation from G2 through prophase and chromosome decondensation from telophase through G1 consistent with experimental observations. An alternative approach, therefore, would be to focus on changes in interphase chromosome structure during cell cycle progression, with the goal of identifying folding intermediates in the pathway of chromosome condensation or decondensation.

Recently, improved visualization of chromatin folding patterns within diploid nuclei and polytene chromosomes was obtained using nonionic detergents in polyamine or divalent cation buffers to remove nucleoplasmic background staining (Bjorkroth et al., 1988; Belmont et al., 1989). In the case of polytene chromosomes, this allowed greatly improved visualization of individual chromatin fibers within a chromosome puff. For diploid nuclei, buffer conditions were chosen which preserved in vitro chromosome morphology, as determined by light microscopy comparison with chromosomes within living cells and by electron microscopy comparison with chromosomes within intact, unpermeabilized telophase cells (Belmont et al., 1989). Using this approach, large-scale chromatin "domains" with 126-nm mean diameter were visualized in both *Drosophila* and human metaphase chromosomes. Examination of semithick sections from anaphase and telophase human chromosomes suggested a looser packing of these domains, while interphase nuclei showed similar size domains within stereopair images (Belmont et al., 1989). These conditions allow use of conventional methods

Address all correspondence to Dr. Andrew Belmont, Department of Cell and Structural Biology, 506 Morrill Hall, 505 S. Goodwin Avenue, University of Illinois, Champaign-Urbana, Urbana, IL 61801. Phone: (217) 244-2311; fax: (217) 244-1648.

for embedding, sectioning, and high contrast staining, facilitating three-dimensional reconstructions from ultrathin serial sections.

In this paper, we exploit this improved visualization to examine the unfolding pathway of interphase chromosomes during progression through G1. We show that a large fraction of chromatin in G1 nuclei is packaged into a higher level folding above the 30-nm fiber consisting of distinct "chromonema" fibers, and we describe cell cycle changes in the conformation of these fibers.

Materials and Methods

Tissue Culture and G1 Synchronization

CHO cells were grown either in Joklik minimal essential medium media supplemented with 10% newborn calf serum (Gibco Laboratories, Grand Island, NY), 1× nonessential amino acids, and 1× vitamin solution, or in F-10 media supplemented with 15% calf serum (Hyclone Laboratories, Logan, UT). Incubation was at 37°C in 5% CO_2.

Two different types of G1 synchronization were used for preparation of electron microscopy samples. A "G1 cycling" synchronization protocol (Burke and Gerace, 1986) used a thymidine block followed by release, a short nocadazole block, and then mitotic shake-off to obtain a mitotic cell population (mitotic index = 98%) that was then plated into small petri dishes. At selected times after mitosis, cells were harvested using trypsin/EDTA. As a control to examine the influence of the thymidine and nocadazole treatments on the morphology of G1 nuclei, separate experiments were done using exponentially growing CHO cultures and mitotic shake-off alone as the synchronization procedure. In this case, mitotic indexes of 84–90% were obtained after 8–10 repeated shake-offs, each separated by 10–15 min.

Alternatively, a "G1-arrested" synchronization method used an isoleucine depletion media to arrest cells reversibly in G1 (Tobey and Crissman, 1972). Cells were plated at 5,000 cells/cm^2 into three 150-cm^2 flasks using F-10 media plus 15% bovine calf serum (Hyclone Laboratories). After 30 h, cells were washed in isoleucine-minus F-10 medium (Gibco Laboratories), and then incubated in isoleucine-minus F-10 plus 10% dialyzed fetal calf serum (Irvine Sci.) for 36 h. Media was then replaced with F-10 plus 15% bovine calf serum supplemented with 1 mM hydroxyurea, and flasks were incubated for 0, 4, or 10 h before harvesting by trypsin/EDTA treatment. Flow cytometry showed that after the isoleucine-minus block, routinely 90–94% of cells were blocked in G1 with the remainder nearly all in the 4c DNA peak (G2 or tetraploid G1). After release followed by 10 h in 1 mM hydroxyurea, flow cytometry showed 93–94% with 2c DNA content, and related experiments showed that this block was reversible for ≥95% of the cells.

Preparation of Samples for Electron Microscopy

Cells in complete medium were pelleted at room temperature, then washed twice in cold isolation buffer. The pellet was resuspended in isolation buffer supplemented with 0.1% digitonin, 0.16% Brij 58, and 0.2 mM PMSF, and then placed on ice. After 5 min, the suspension was washed and resuspended in cold isolation buffer. Aliquots were pelleted in Eppendorf tubes at low speed for specimen embedding.

The isolation buffer, buffer A, consisted of 80 mM KCl, 20 mM NaCl, 2 mM EDTA, 0.5 mM EGTA, 15 mM Pipes buffer, 15 mM beta-mercaptoethanol, 0.5 mM spermidine, 0.2 mM spermine, and 10 μg/ml turkey egg white protease inhibitor (Sigma Immunochemicals, St. Louis, MO), adjusted to pH 7.0.

Fixation was with 2% glutaraldehyde in buffer A for 12 h at 4°C. As discussed previously (Belmont et al., 1989), because of the polyamines present in the buffer, the glutaraldehyde was added in small increments directly to the cell suspension or the supernatant over the cell pellet using an 8% glutaraldehyde solution. This gave a 3:1 buffer/8% glutaraldehyde solution. After three 5-min washes in buffer A without beta-mercaptoethanol, samples were postfixed in 1% osmium tetroxide for 1 h on ice.

Embedding, Sectioning, and Section Staining

Dehydration, infiltration, and embedding in Epon 812 were carried out as described previously (Belmont et al., 1989). Thin sections were cut with a Standard Diatome diamond knife (Diatome), and semithick sections 0.2–2.0 μm thick were cut with a Semi Diatome diamond knife using an Ultracut E ultramicrotome (Reichert Jung, Vienna, Austria). Sections were placed onto formvar-coated grids. Serial thin sections, ranging in thickness between given data sets from 30 to 85 nm, were collected onto slot or single hole grids. Grids were stained from both sides with 0.2% uranyl acetate in 50% EtOH, poststained in 0.02% lead citrate, and carbon coated.

Electron Microscopy and Data Collection

Sections were examined at 60–100 kV on a transmission electron microscope (TEM) (100C; JEOL U.S.A. Inc., Peabody, MA).

An Eikonix 1412 camera, capable of 12-bit grey scale readout of a 4,096-pixel linear detector array, was used with a Gordon model 5 × 5 Plannar light source (Gordon Instruments, Orchard Park, NY) to digitize negatives using software developed in the laboratory for a DEC Microvax 3200. 1,024 × 1,024 areas were scanned, with correction for individual pixel variations in gain and dark current, and flat-fielding correction for variations in light intensity over the area of the light box.

A "mass normalization" procedure to convert film optical density values to values proportional to the integrated scattering cross-section, or electron optical density, was carried out as described previously (Belmont et al., 1987). Image "intensity" values then reflect the density of heavy metal staining, with brighter regions corresponding to higher electron density as in a negative. For thin serial sections (30–40-nm), the background intensity varied across the cell nucleus, producing variations in density in the images produced by the above method. For these thin sections, therefore, a variation of the above "mass normalization" procedure was used. Rather than using the overall background peak as the background value for the entire image, a low pass filter was applied to the image. The background value used for a given pixel was then made equal to the value at the same pixel in the low pass filtered image. This procedure produced flat uniform normalization of density values at the expense of reducing the mean intensity of large regions with uniform density, such as nucleoli.

Alignment of serial sections was accomplished by one of two methods. 70–85-nm thick sections, in which the correlation between adjacent sections was poor, but for which the elastic section compression was minimal, were aligned using a procedure minimizing the minimum distance between equally spaced points on corresponding contours from adjacent sections (Belmont, A. S., manuscript in preparation); for interphase nuclei, the nuclear envelope and nucleolus borders were used as contours, while for mitotic cells, the contours from three to four different chromosomes were used. A modified quadratic interpolation was used for the image transformation. Thinner sections, in which the correlation between adjacent sections was better but elastic deformation of the sections was worse, were first roughly aligned using the method described above. Selected subvolumes were then realigned using a cross-correlation alignment procedure in which a normalized cross-correlation was computed and minimized as a function of a general linear affine transformation, which includes nonuniform, but linear, shrinkage and shear (Belmont, A. S., manuscript in preparation).

Preparation of Samples for Light Microscopy

A G1-arrested synchronization used the same protocol as described above, with the cells plated directly on coverslips. At 0 to 10 h release from the isoleucine block, cells were fixed using glutaraldehyde. Coverslips were rinsed briefly in calcium- and magnesium-free PBS (CMF-PBS)[1], and then incubated in CMF-PBS with 1% glutaraldehyde for 10 min at room temperature. Fixation was continued for 12 h at 4°C. Coverslips were then washed in CMF-PBS and stained with 0.5 μg/ml 4'6-diamidinophenylindole, dihydrochloride (DAPI).

Alternatively, G1-synchronized cells were obtained using a nocadazole block followed by selective detachment as described above. However, no previous thymidine block was used, and the cells were cultured in F-10 plus 15% calf serum. Fixation and staining used CMF-PBS as described above.

Deconvolution Light Microscopy

A conventional inverted light microscope (IMT-2; Olympus) equipped with a Photometrics cooled, slow-scan charge-coupled device camera was used. This system duplicates one built by Drs. Agard and Sedat (University of

1. *Abbreviations used in this paper*: CMF-PBS, calcium- and magnesium-free PBS; DAPI, 4'6-diamidinophenylindole, dihydrochloride.

California at San Francisco), and it has been described elsewhere (Hiraoka et al., 1991). Briefly, it includes motorized filter wheels for excitation and emission filters (Omega Optical) and a microstepping motor for z-focus, with a Silicon Graphics 4D/35TG computer providing automated data collection using the Resolve3D data collection program (Applied Precision). A 60×, 1.4 NA Plan Apo oil immersion lens (Olympus) was used together with narrow-pass filters for DAPI excitation and emission. Optical sections were collected through entire nuclei at 0.2-μm focal intervals; pixel size was 0.074 μm, and 512 × 512 pixel images were taken. Deconvolution of optical sections, to partially restore the image degradation resulting from out-of-focus blur, was accomplished using an enhanced ratio, iterative constrained deconvolution algorithm (Agard et al., 1989).

Image Display

The display program, NEWVISION (Pixton, J., and Belmont, A. S., manuscript in preparation), running on an SGI 4D/35 TG was used to display images and view results. Selected images or montages were then assembled into figures using Adobe Photoshop (Adobe Systems Inc., Mountain View, CA). Figures were printed using a Colorstream printer from Mitsubishi Kasei Corp. (Tokyo, Japan).

Results

Cell Cycle Synchronization

For preparation of EM samples, we used two methods for synchronizing cells in G1. A G1 cycling synchronization protocol (Burke et al., 1986) used release from an S phase block, followed by a brief mitotic block and then mitotic shake-off to obtain mitotic cells. After shake-off, these cells were incubated for 1, 2, or 3.75 h before fixation and specimen preparation for electron microscopy. Mitotic indexes routinely were ≥98%, and decondensation events appeared similar to those observed in control experiments that used mitotic shake-off of unsynchronized cultures and achieved mitotic indexes of 84–90%. BrdU labeling showed DNA synthesis beginning after 2 h with the labeling index reaching 40% at 4 h (data not shown), consistent with previous measurements (Lloyd et al., 1982).

A second G1 arrest synchronization method used an isoleucine depletion media to arrest cells reversibly in G1 (Tobey et al., 1972). Cells were then released into G1 and allowed to progress through G1 and accumulate at G1/S by addition of normal media supplemented with hydroxyurea. In this case, time points of 0, 4, and 10 h after release were used for sample preparation. Flow cytometry showed 90–95% of cells with 2c DNA content (data not shown). Previous work using this cell synchronization method without hydroxyurea treatment has shown that the labeling index (percentage of cells in S phase) begins to rise at ~5 h after release from the isoleucine-minus block reaching near 100% between 10 and 12 h (Tobey et al., 1970).

For light microscopy, we used similar synchronization protocols. However, for the G1 cycling method, we skipped the previous thymidine block and we grew the cells in a less rich media, F-10, to lengthen slightly the G1 period and to obtain a finer division of early G1 decondensation events.

General Overview of G1 Chromatid Decondensation by Optical Sectioning Light Microscopy

Cells synchronized by both the G1 cycling and G1-arrested synchronization protocols were examined using deconvolution, optical sectioning light microscopy. A computer-controlled, wide-field microscope equipped with a cooled slow scan charge-coupled device camera was used to collect complete through-focus series of entire nuclei from DAPI-stained cells. The focus interval was 0.2 μm, and data from 40–100 focal planes was collected for each data set. Out-of-focus blurring was reduced through use of an iterative constrained deconvolution algorithm.

Results from this light microscopy survey demonstrate several points.

First, a continuous overall process of chromatid decondensation is visualized between telophase and early G1, although along the length of a particular chromosome, chromatid decondensation is highly nonsynchronous. As reported previously (Enger et al., 1968), anaphase in this system begins ~20 min after release from the mitotic block. At the first time point shown in Fig. 1, 40 min, cells are mostly in various stages of telophase. Chromosomes are difficult to visualize because of their compaction and close contact within the characteristic hemispherical shell-shaped conformation of telophase nuclei (Welter et al., 1985; Hodge et al., 1990). However, in late anaphase/early telophase, they can be traced as continuous condensed chromatids with 0.4–0.6-μm diameters as shown in Fig. 1, *A* and *B*.

In later stages of telophase and early G1 visualized in the 1-h time point, recognizable chromatids are fewer in number, but examples can still be identified and traced as in Fig. 1, *C* and *D*; in many cases, their diameter is now reduced to ~0.2–0.3 μm. There appears to be a range of nuclei in different stages of decondensation, as measured by the reduced number and average length of these decondensed chromatid regions. At still later times, nuclei are present with many small isolated segments. Because of this apparent continuum in decondensation, these short condensed regions in early G1 nuclei most likely represent chromosomal segments that are the most delayed in decondensation, and we will refer to them as "G1 chromatids." With further time, many nuclei appear in which small condensed spots are present throughout the nucleus, but with few or none of the larger linear segments remaining.

Second, concurrent with the decondensation of these condensed chromatids is the appearance of a much finer, apparently fibrillar DNA substructure within the nucleus. In later stages of G1, as in the 4-h time point from the G1 cycling method or 10 h in the G1-arrested synchronization, the majority of the DAPI staining appears to be represented in this fibrillar pattern that is now distributed throughout most of the nuclear interior. Examples are shown in Fig. 1, *E* and *G*. This pattern of staining is similar to that observed previously in living HeLa cells stained with Hoescht 33342 (Belmont et al., 1989), although the apparent fibrillar nature of the staining is even more accentuated; this is likely a combined result of the longer exposures and more complete optical sectioning and deconvolution approaches made possible by working with fixed samples. Moreover, a similar appearance was observed, whether cells were fixed with glutaraldehyde in PBS buffer as in Fig. 1, or after permeabilization in the polyamine buffer A (data not shown). Previous work correlating light and electron microscopy observations on the same nucleus in thin Epon sections demonstrated that this apparent fibrillar fluorescence staining pattern corresponded by electron microscopy to distinct large-scale domains ~80–130 nm in width (Belmont et al., 1989).

Third, similar fibrillar substructure is apparent in the deconvolved optical reconstructions in regions of local chro-

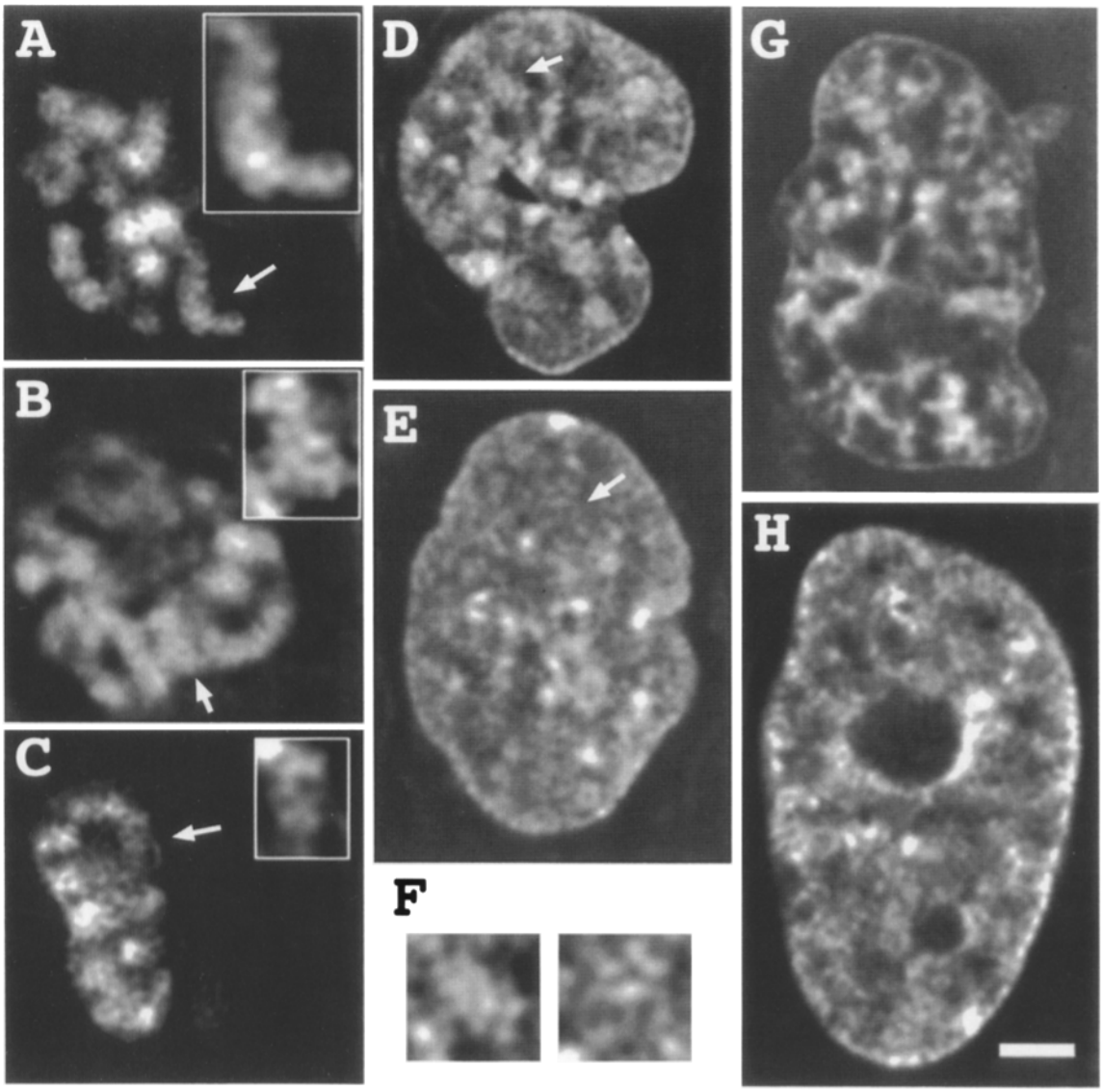

Figure 1. Light microscopy survey of G1 chromatid decondensation. (*A–B*) Individual optical sections shown at two different focal planes for two daughter nuclei in early telophase (40 min after mitosis). Arrows point to regions enlarged twofold in boxed regions. Note the substructure present within the chromatid arms (see text). (*C*) Optical section from later in telophase. Chromatids, associated closely with the nuclear envelope, are still recognizable but cannot be easily traced over extended distances. Boxed area shows region of local decondensation where substructure, consistent with fibrillar folding, is present. (*D*) Early G1 nucleus, 1.5 h after mitosis. Short segments of local condensed regions similar in appearance to the chromatids from telophase nuclei are present (see arrow and twofold enlargement in *F*). Also present are linear, condensed regions of reduced width (0.2–0.3 μm diameter; see region below arrow). (*E*) Decondensed nucleus, 4 h after mitosis. The majority of chromatid is now dispersed through the nuclear interior. Substructure within nucleus is similar in size to that contained within the condensed chromatids visualized in telophase and early G1 and is suggestive of an underlying fibrillar substructure. (*F*) Twofold enlargements of regions, marked by arrows, in *D* and *E*. (*G*) G1-arrested nucleus showing condensed chromatid-like regions (*H*) late G1/early S phase nucleus (hydroxyurea-treated cells, 10 h after release from isoleucine minus G1 arrest). Bar, 2 μm (1 μm for enlarged regions).

matin condensation. This substructure is increasingly apparent as the overall level of condensation decreases in the transitions between telophase chromatids, the G1 chromatids described above, and local areas of high packing density as visualized in regions of early G1 nuclei. Overall, the observed results are suggestive of a continuous decondensation of G1 chromatids and condensed chromatin masses through a progressive unraveling of some underlying substructure. Examples are shown in Fig. 1, *A–F*.

Fourth, the overall pattern of decondensation after release from the isoleucine-minus G1 arrest parallels to a large extent that described above for G1 progression after mitosis. G1-arrested nuclei show condensed chromatin regions similar to those visualized in early G1 cells; progression after release from this block is associated with a disappearance of these condensed regions, and a dispersed, apparent fibrillar staining pattern typical of late G1 nuclei as shown in Fig. 1, *G* and *H*.

Early G1 and G1-arrested Nuclei Show Peripheral Chromatin Distribution at Various States of Condensation: Condensed Chromatid-like Regions Coexist with Extended Chromonema Fibers

Closer examination of decondensation events observed by light microscopy was provided by survey electron micrographs of semithick Epon sections (0.2 μm thick). We used cells permeabilized with detergent in the polyamine buffer A. As discussed previously, this provided improved visualization of the large-scale chromatin domains, while preserving the overall folding patterns of these large-scale chromatin domains, as assayed by correlative light and electron microscopy, as well as by comparisons by light and electron microscopy of permeabilized vs nonpermeabilized cells (Belmont et al., 1989). Because the uranyl/lead staining was nonselective for DNA, we concentrated on the condensed G1 chromatids described earlier and the fiberlike large-scale chromatin domains, >60 nm in width, which again had previously been shown to correspond to the fibrillar DAPI staining patterns visualized in Fig. 1 (Belmont et al., 1989).

Compared to log phase populations, nuclei from these synchronized populations were quite homogeneous in appearance as documented later in this paper (see Fig. 9, Table I). The overall pattern of decondensation paralleled closely the general trends inferred from the light microscopy results described above. Representative examples from 1 h after mitosis and after G1 arrest are shown in Fig. 2. At 1 h after mitosis, a large fraction of chromatin is distributed within a roughly 1-μm shell surrounding the nuclear envelope and nucleolus. At this stage, the extent of chromatid decondensation is highly heterogeneous. Condensed chromatin regions, 0.2–0.4 μm in width, reflecting chromatid regions late in decondensation, are present throughout the nucleus. A large fraction of the remaining chromatin appears packaged in 100–130-nm diameter chromatin domains that are mostly coiled within local regions. In a few areas, though, extended, spatially distinct 100–130 chromatin domains can be visualized. As we demonstrate later in this paper, these large-scale chromatin domains in fact correspond to actual fibers that we will refer to as "chromonema" fibers to distinguish them from lower order 10- and 30-nm chromatin fibers.

After G1 arrest by growth in isoleucine-minus media (0-h release), nuclei have a distinctive appearance similar in some respects to the early G1 nuclei. Like at 1 h after mitosis with the G1 cycling synchronization method, most chromatin appears concentrated near or adjacent to the nuclear envelope or nucleoli, with locally condensed regions $\leq$0.4 μm in diameter again obvious. Several features, however, distinguish these nuclei from the early G1 nuclei. Nucleoli are larger and more prominent, and there is a much greater heterogeneity in chromatin condensation patterns. A significant fraction of the chromatin is also present as extended fiberlike 100–130- and 60–80-nm chromatin domains, more typical of later G1 nuclei. Frequently, chromonema fibers are present as extended fibers stretching 1–2-μm between the nuclear envelope and nucleolus surfaces, or between either of these surfaces and the periphery of interchromatin granule clusters.

A second difference is that the overall intranuclear chromatin distribution is also more heterogeneous than in the early G1 nuclei. Large areas completely devoid of uranyl/lead staining are present within the nuclei, and the condensed chromatin regions are more tightly opposed to the nuclear envelope and nucleoli surfaces. Aside from chromonema fibers associated with nucleoli and interchromatin granule clusters, very little chromatin appears present within the nuclear interior. The relationship of the G1 arrest in these CHO cells, a transformed cell line, to the G0 arrest state of nontransformed cells is not entirely clear. However, we expect that this observed appearance of the G1-arrested nuclei may be related to the more extreme disappearance of internal nuclear matrix staining seen in terminally differentiated erythrocyte nuclei (Lafond and Woodcock, 1983), and the decreased nonhistone protein content, including reduction of topoisomerase 2 alpha (Heck and Earnshaw, 1986), seen in nuclei from some nonproliferating cells.

Early G1 and G1-arrested Chromatids Contain 100–130-nm Chromonema Fibers

As the next stage of analysis of the large-scale chromatin organization of these G1 nuclei, we assembled four to five serial section data sets from each time point. Each data set corresponded to a different nucleus and consisted of between 20 and 90 serial sections. A few early data sets had section thickness of 80 nm. Improvements of our alignment algorithm allowed us to compensate for the elastic deformation associated with sectioning, particularly that of very thin sections. Therefore, the remaining data sets were cut at section thicknesses ranging from 30 to 40 nm.

Serial section reconstructions of early G1 nuclei demonstrated that many of the condensed chromatin masses visualized within individual sections in fact correspond to extended linear structures in three dimensions. The light microscope survey of early G1 described above indicated a continuous process of chromatid decondensation that continued after telophase, although chromatid decondensation was highly nonsynchronous along the length of the chromosome. Therefore, these condensed, linear regions most likely represent chromosomal segments that are the most delayed in decondensation, and we will refer to them as G1 chromatids. Similar regions could also be visualized within the G1-arrested nuclei.

Fig. 3 shows several examples of these regions. Each panel row contains a projection or sum of multiple serial sections followed by individual serial sections. Because of space limitations, only a subset of the serial sections forming the projection could be shown; these were chosen to illustrate specific points. Note that the accuracy of our alignment procedure is excellent; at this magnification, we find our projections of serial sections similar to intermediate voltage electron micrographs of semithick physical sections. Based on simulated tests of our algorithm and analysis of actual serial section reconstructions, we estimate our alignment accuracy to be on the order of one pixel or better (7–12 nm for the reconstructions shown in this paper). This accuracy allows us to connect sections of an individual chromonema fiber between adjacent sections.

In all three examples, fiberlike features 100–130 nm in width, as marked by arrows, are prominent components of the overall structures. Because of the tight coiling and close packing of these features, the separation between these objects is in most places smaller than the section thickness, preventing a clear demonstration that these features cor-

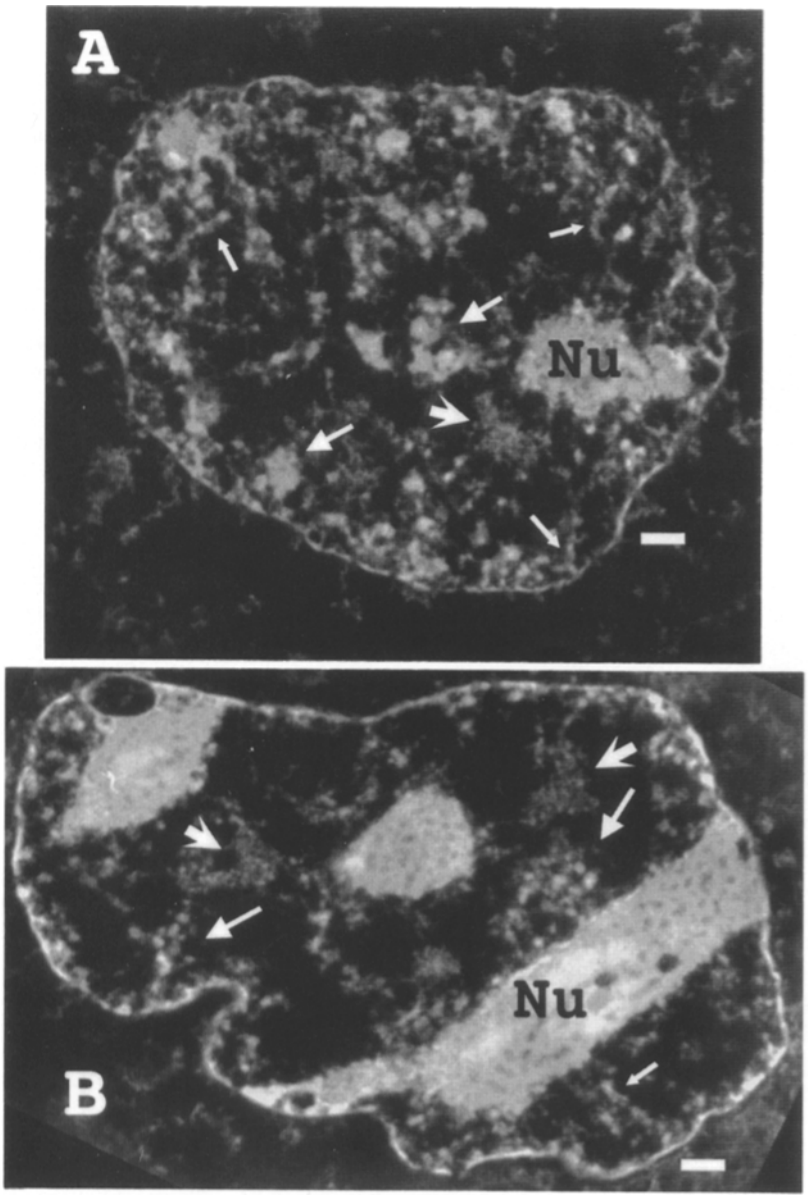

Figure 2. Early G1 and G1-arrested nuclei (0.2 μm semithick sections). All electron micrographs are displayed with reverse contrast as in a negative; heavily stained regions appear white. (*A*) Nucleus, 1 h after mitosis. Condensed chromatin is concentrated near nuclear envelope. Large arrows point to condensed chromatid-like regions, 0.2–0.4 μm in width. Small arrows point to individual "chromonema" fibers, 0.1–0.13 μm in diameter (see text). (*B*) G1-arrested nucleus (isoleucine-minus block). Condensed chromatin masses (*large arrows*), as in early G1 nuclei, are concentrated near nuclear envelope and adjacent to nucleolus (*Nu*). These regions appear to be formed by tight folding of 0.1–0.13-μm diameter "chromonema" fibers. Individual chromonema fibers are also present (*small arrow*). Curved arrowheads (*A* and *B*) point to interchromatin granule clusters. Bar, 0.5 μm.

respond to actual fibers. However, in two locations in Fig. 3 *A*, an isolated 130-nm fiber connecting more condensed regions can be shown by serial sections to correspond to an actual fiber; in both cases, these extended segments of 130-nm fibers appear to lead into a sharp kink of the fiber. Fig. 3 *B* shows two apparent supercoiled loops formed by these fibers.

An example from a G1-arrested nucleus in Fig. 4 *A* shows a slightly less condensed folding of 100–130-nm chromonema fibers. In this case, locally condensed regions formed by the apparent tight folding of 100–130-nm fibers are connected by what serial sections reveal is a 100–130-nm diameter fiber.

Examples from early G1 nuclei of small condensed chromatin regions formed by the apparent kinking and tight coiling of similar 100–130-nm chromonema fibers are shown in Fig. 4, *E–J*. Fig. 4, *K–N* show an example of a supercoiled loop formed by the relational coiling of a 100–130-nm chromonema fiber about itself.

G1 Progression is Associated with a Dispersal of Chromatin throughout the Nuclear Interior, Loss of Condensed Chromatid-like regions, and an Uncoiling and Decondensation of Chromonema Fibers

At later time points in G1, again the overall pattern of decondensation paralleled closely the general trends inferred from light microscopy results. As shown in Fig. 5 *A*, by 2 h after mitosis, the chromatin is now distributed throughout the nuclear interior, with large condensed chromatin regions now smaller and rarer. More common are small regions of condensed chromatin that appear to correspond to local kinks and coils of a 100–130-nm chromonema fiber, similar to the serial section examples shown in Fig. 4. While these 100–130-nm chromatin domains still make up a large fraction of the total chromatin, they are present as straighter, shorter segments dispersed more evenly through the nuclear interior. At the last time point examined, 3.75 h after mitosis, the chromatin distribution is even more homogeneously dis-

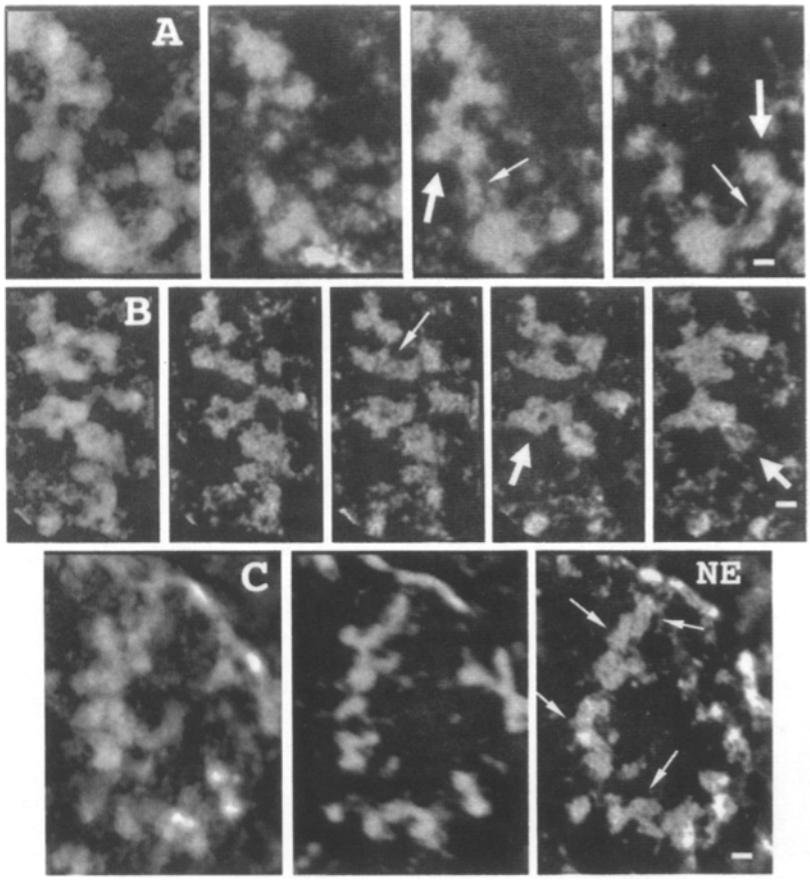

Figure 3. Early G1 and G1-arrested chromatids contain 100–130-nm chromonema fibers. (*A–C*) Projections through multiple adjacent serial sections of selected regions from G1 (*A* and *B*) and G1-arrested nuclei (*C*), with panels to right showing individual serial sections. (*A*) Projection through 4, 85-nm thick serial sections (*left*) and three adjacent serial sections. Thick arrows point to kinks formed by relational coiling of 100–130-nm diameter fibers. Thin arrows point to segments of 100–130-nm diameter "domains" which by comparison of adjacent serial sections can be demonstrated as corresponding to actual large-scale chromatin, or chromonema, fibers. (*B*) Projection formed by 6, 35-nm thick serial sections (*left*), and the middle four adjacent serial sections. Thick arrows point to apparent supercoiling of 100–130-nm diameter fibers; thin arrows point to the isolated segment of a 100–130-nm diameter fiber. (*C*) Projection through 8, 40-nm thick serial sections (*left*) and two adjacent serial sections showing internal 100–130-diameter fiber-like features (*arrows*). Bars, 120 nm.

tributed through the nuclear interior, few if any large condensed chromatin regions are present, and 100–130-nm diameter fibers are rarer and appear mostly as short segments. Instead, the chromatin packing is significantly more decondensed with thinner 60–80-nm diameter chromonema fibers distributed throughout the nucleus.

A similar trend is observed for chromatin decondensation after release of G1 arrest by isoleucine deprivation. A second block in early S phase by hydroxyurea treatment results in nuclei that appear maximally decondensed relative to all other time points examined from either synchronization method. Fig. 5 *B* shows an example in which few condensed chromatin masses can be visualized. Instead, large-scale chromatin fibers, mostly 60–80 nm in diameter, appear distributed throughout the nuclear interior. These 60–80-nm chromonema fibers are now frequently present as straight extended fibers that can be traced for 1–2 μm in areas of these semithick survey sections.

Particularly prominent in Fig. 5 *B* are several interchromatin granule clusters. These have a distinctive morphology, as described in the literature, consisting of a dense central region containing roughly 20-nm granules, frequently clustered into linear chains, surrounded by a shell of fibrillar material, or perichromatin fibrils (Spector, 1993). Interchromatin granule clusters are thought to represent storage areas for splicosome components, and it has been proposed that the dense central region with its granules are the actual storage area for splicosome components, while the perichromatin fibrils distribute these components to transcriptionally active sites (Spector, 1993). Some but not all transcriptionally active genes appear to be associated at the periphery of these structures (Xing et al., 1993). These interchromatin granule clusters measure ~0.5–2.0 μm in diameter and can be recognized at all cell cycle stages examined. They appear to be larger in these early S phase, hydroxyurea-arrested nuclei.

Chromonema Fibers can be Traced in Serial Sections as Individual Extended Fibers Measuring 0.5–2.0 μm in Length

In early G1 nuclei, examples where 100–130-nm diameter "chromonema" fibers can be traced as distinct fibers for lengths of 0.5–1.0 μm are present but not abundant. Most of the chromatin in these nuclei appears to be present as 100–130-nm chromonema fibers too tightly coiled to be traced unambiguously as distinct fibers by our serial section reconstructions. Therefore, it is likely that 0.5–1.0 μm is an underestimation of maximal fiber length. As described above, with G1 progression, large-scale chromatin packing shows an overall decondensation that includes an extension or straightening of these chromonema fibers simultaneous with a dispersion of these fibers throughout the nuclear interior. These changes greatly facilitate the tracing of individual fibers using serial sections and allow us to find examples where extended chromonema fibers are oriented nearly parallel to the plane of section and can be traced in just several sections.

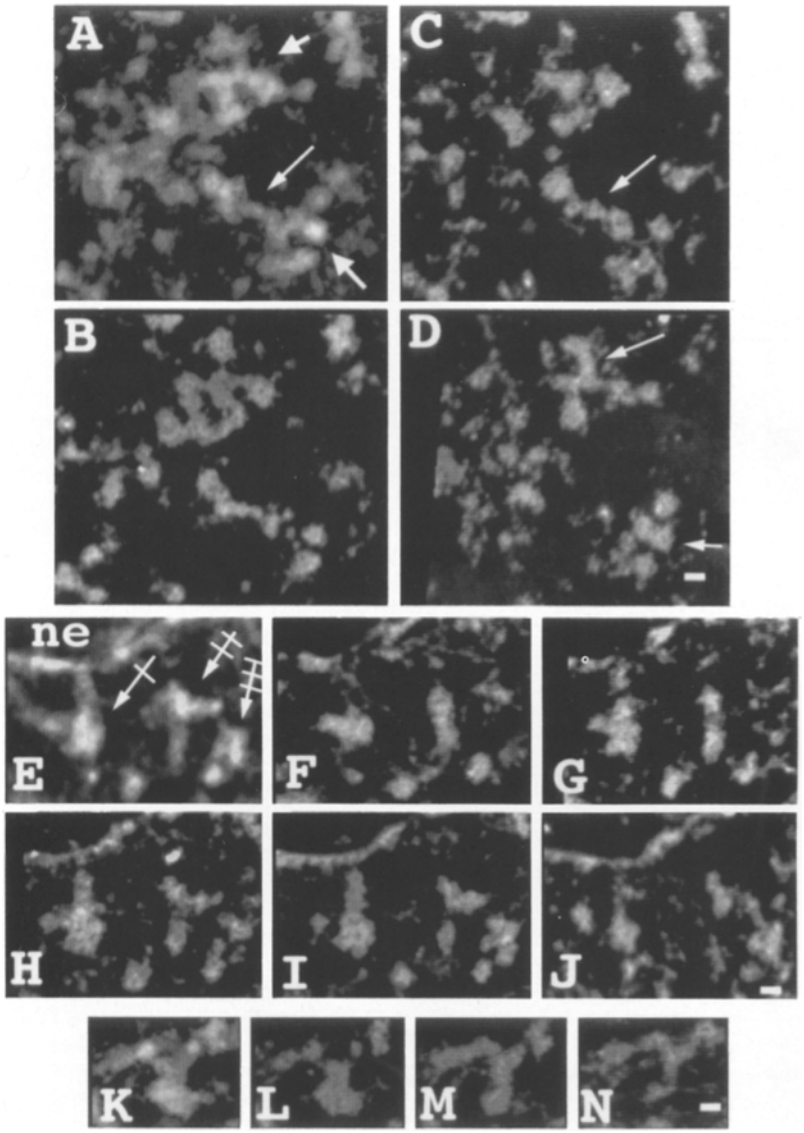

Figure 4. Small condensed regions more clearly demonstrate local folding and kinking of 100–130-nm chromonema fibers: (*A–D*) A condensed region from a G1-arrested nucleus. (*A*) Projection through 10, 40-nm thick sections, (*B–D*) individual serial sections at positions 2, 4, and 7 in the stack of 10. Two locally condensed regions (*thick arrows*, *A*) are connected by individual chromonema fiber (*thin arrow*, *A*). Adjacent serial sections not shown demonstrate that this is an actual fiber. Thin arrows in *D* point to similar size features within the condensed regions, suggesting that these condensed regions are formed by folding of chromonema fibers. (*E–J*) and (*K–N*) show regions from early G1 nuclei, 1 h after mitosis. (*E*) Projection through 10, 35-nm thick serial sections, and (*F–J*) individual serial sections from positions 1, 2, 3, 4, and 6 in the stack of 10. Three locally folded regions in *E* are marked by arrows with 1, 2, or 3 cross-hatches. One cross-hatch arrow marks area where an individual chromonema fiber descends vertically from nuclear envelope (*H–I*), kinks sharply (*G–I*), folds horizontally towards left across original fiber (*F–G*), and then curves upwards, perpendicular to the sectioning plane (*I–J*). Two cross-hatch arrow marks chromonema fiber that makes abrupt 90° bend (*H–I*). Three cross-hatch arrow points to local condensed region apparently formed by tight folding of a similar chromonema fiber (*H–J*). Note that the second and third regions appear to be connected by a thinner decondensed fiber (*J*). (*K*) Projection through 6, 35-nm thick serial sections. (*L–N*) adjacent serial sections show a horizontal chromonema fiber (*left*) apparently supercoiling vertically into a relational coil that then exits horizontally (*right*). Bars, 120 nm.

Figs. 6 and 7 show examples of such chromonema fibers that can be traced as distinct fibers over distances from 1 to 2.5 μm in length. Fig. 6 *A* shows a fiber consisting of several 100–130-nm diameter segments, each 0.5–1.0 μm in length, which appear connected at localized constrictions; these constrictions appear to contain loose folding of individual chromatin fibers connecting the individual chromonema fiber segments. This fiber is attached to the left at the edge of a nucleolus where it reverses direction. Similar examples of 100–130-nm fibers are shown in Fig. 6, *B–C*. In Fig. 6 *B*, the fiber appears to coil in a tight corkscrew over much of its length and attaches at one end to the nuclear envelope.

Attachment of these chromonema fibers to the nuclear envelope is a prominent feature at all time points in G1, and additional examples can be seen in Figs. 2–5 and 7. Examples can be found in which these chromonema fibers are tightly attached to the nuclear periphery over extended lengths, as well as cases where the chromonema fibers can be traced through a local attachment; loops formed by extended chromonema fiber lengths with both ends attached at nearby sites on the nuclear periphery are also present (data not shown). Recently, we showed that these local attachments of chromonema fibers at the nuclear periphery interact with the nuclear lamina; heavy concentrations of lamin B directly "cap" the surface of envelope associated chromonema fibers (Belmont et al., 1993).

Chromatin Decondensation Is Associated with a Transition from 100–130- to 60–80-nm Diameter Chromonema Fibers

As described earlier, there is also a decrease in diameter of these chromonema fibers associated with G1 progression. At any given time point, there are chromonema fibers with diameters of 60–80 and 100–130 nm; however, at early time points, most chromonema fibers are 100–130 nm, while at late G1 and early S time points, most chromonema fibers are 60–80 nm in diameter. A priori there are two possibilities for these diameter variations. First, there may be a continuous distribution in fiber diameter that shifts towards lower diameter with G1 progression. However, subjective analysis of numerous semithick survey sections and serial thin sec-

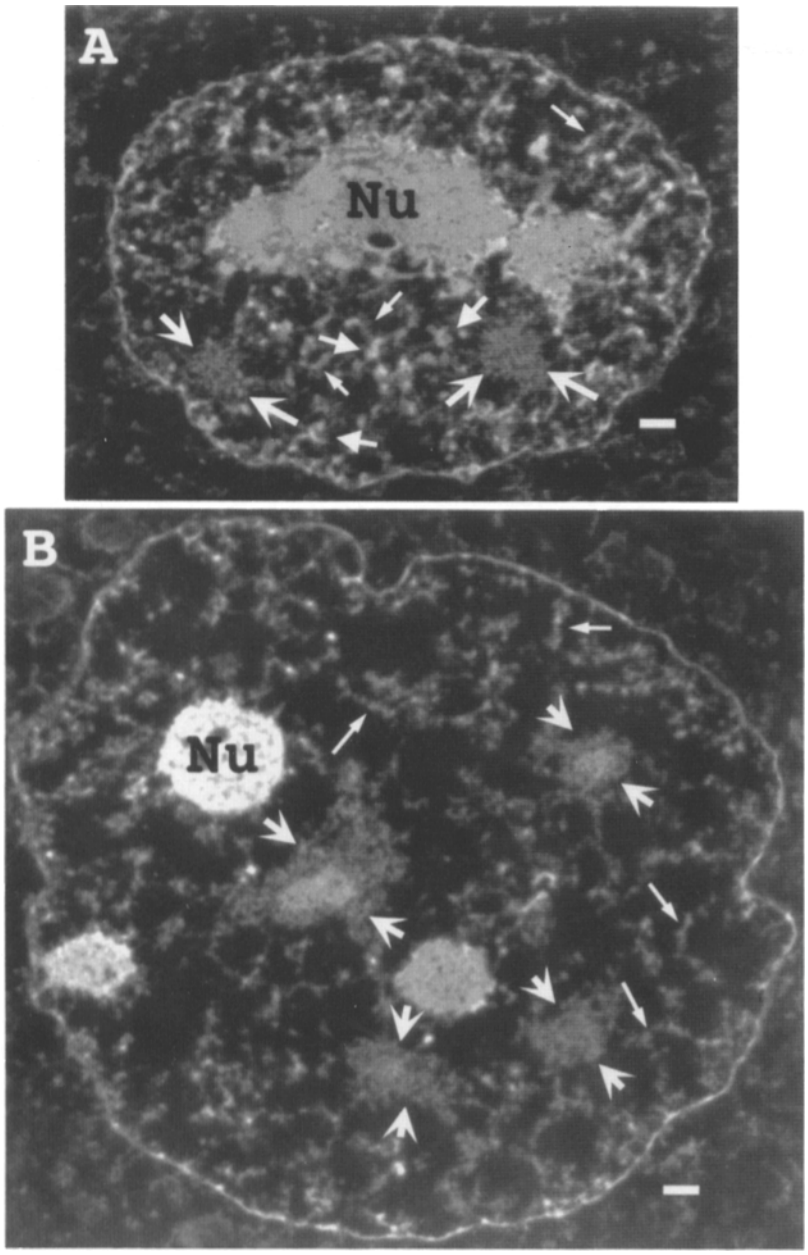

Figure 5. Middle and late G1 nuclei (0.2-μm semithick sections). (*A*) G1 nucleus 2 h after mitosis. Chromatin is now dispersed throughout nuclear interior. 0.5–1.0-μm long segments of 100–130-nm diameter chromonema fibers are prominent (*thin arrows*). Thicker arrows (*flat arrowheads*) point to small condensed chromatin regions formed by local tight coiling and kinking of these fibers. (*B*) Late G1/early S phase nucleus (S phase block after release from G1 arrest). Chromatin is highly dispersed and decondensed. Extended 60–80-nm diameter chromonema fibers (*thin arrows*) are now dominant. Many can be followed as extended fibers over 2–3-μm distances. Arrows with curved arrowheads (*A* and *B*) mark interchromatin granule clusters. *Nu*, nucleoli. Bars, 0.5 μm.

tions has suggested to us that there are in fact two distinct size classes of chromonema fibers rather than a continuous distribution. The second possibility, therefore, is that the 100–130-nm chromonema fibers directly unfold into the 60–80-nm chromonema fibers. In principle, this could occur through a complete structural reorganization of the underlying chromatin fibers. Alternatively, the 100–130-nm chromonema fiber may itself be formed by the folding of an underlying 60–80-nm chromonema fiber, with G1 progression associated with an uncoiling of this underlying 60–80-nm chromonema fiber.

Definitive resolution of these two possibilities is technically difficult. One obvious beginning step would be to develop methods for quantitative and objective measurements of fiber widths, and to use these to produce histograms of fiber widths as a function of cell cycle stage. Because of three-dimensional folding of fibers and the variation in width along each individual fiber, this is a nontrivial and time-consuming task, particularly to obtain sufficient numbers of measurements for statistically meaningful results. It is further complicated by the bias resulting from the practical restriction of measurements to extended fibers. Instead, work in progress is focused on using higher resolution EM tomography reconstruction techniques together with methods of identifying specific chromosome regions as a means of analyzing this transition for a defined genomic region.

However, in Fig. 7, we present several examples suggestive of the second possibility in which the 100–130-nm chromonema fibers unfold directly into 60–80-nm chromonema fibers. In Fig. 7, *A–D*, a single chromonema fiber can be traced as a continuous fiber for ~2.5 μm, stretching from the edge of a nucleolus to the edge of an interchromatin gran-

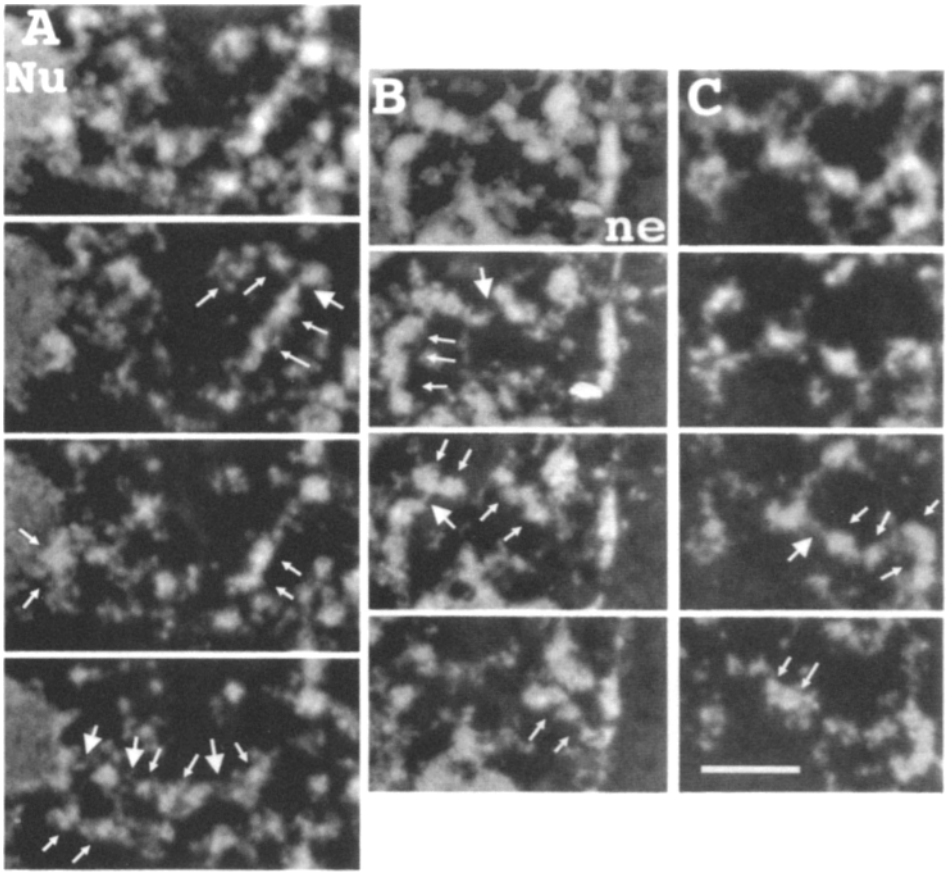

Figure 6. Chromonema fibers can be traced as distinct fibers for 1–3 μm: Three examples (*A–C*) of well-isolated, extended chromonema fibers running roughly parallel to the sectioning plane. Top panels show projections through several serial sections; below are individual serial thin sections. Small arrows mark the path of these fibers in the individual sections. Larger arrows point to regions where segments of chromonema fibers are connected through locally decondensed regions. (*A*) Approximately 3-μm-long fiber with several sharp bends, and an attachment (*left*) to the edge of a nucleolus (*nu*). (*B*) Fiber consisting of three condensed segments, 100–130 in nm diameter, connected by two locally decondensed regions. There is a corkscrewing of the fiber apparent particularly at the right hand side of the figure, near where the fiber makes contact with the nuclear envelope (*ne*). (*C*) Extended fiber consisting of several condensed segments connected by locally decondensed regions. Bar, 0.5 μm.

ule cluster. Individual serial sections demonstrate several sharp transitions from 60–80-nm diameter fibers to short segments that are 100–130 nm in width. Fig. 7, *E–G* shows three fibers in which there is an abrupt transition in diameter from 100–130 to ~80 nm.

Local Decondensation of Chromonema Fibers

At early time points in G1 or release from G1 arrest, there is great heterogeneity in the overall large-scale chromatin packing. Condensed G1 chromatid regions coexist with isolated 100–130-nm chromonema fibers. As discussed earlier, we speculate that these late decondensing regions are related to late-replicating heterochromatin regions of the genome, and experiments are in progress to test these ideas.

There is also heterogeneity in large-scale chromatin packing on a more local scale. At middle to late G1 time points, there is the variation in chromonema fiber diameter already discussed in the previous section. Sudden transitions between 100–130- and 60–80-nm diameter fibers were illustrated in Fig. 7. Also seen in these nuclei are local regions where chromonema fibers are further unfolded.

Fig. 8, *A–C* shows an extended region in which short segments of chromonema fibers, or islands of condensed chromatin are connected by more loosely folded regions that appear to contain folded 30-nm chromatin fibers. Fig. 8 *D* shows a single thin section that contains an extended chromonema fiber. In two regions, this chromonema fiber shows a local transition to what appears to be loose coiling of a 30-nm chromatin fiber. Interestingly, in one of these regions, there is a short segment that is surrounded by diffuse fibrillar material; we speculate that this may represent a local accumulation of RNPs surrounding a site of transcription. As mentioned earlier (see Fig. 7 *A*), chromonema fibers frequently appear associated with the edge of interchromatin granule clusters. In a number of cases, we see local decondensation of these chromonema fibers at the edges of these interchromatin granule clusters; Fig. 8 *E* illustrates one example of this local unfolding. This local decondensation exactly in the region of association with the interchromatin granule cluster is intriguing, given recent results in the literature demonstrating association of specific transcriptionally active genes at these interchromatin granule clusters, or "splicosome islands" (Xing et al., 1993). Finally, Fig. 8 *F* shows a loop of local unfolding connecting at both ends with condensed 100–130-nm chromonema fibers. One end of this loop appears connected with the condensed, chromonema fiber by an extended 30-nm chromatin fiber.

If we assume a 36:1 packing ratio for the 30-nm chromatin fiber, then the short segments of extended 30-nm chromatin fibers seen, for instance, in Fig. 8, *D* and *F* correspond to ~25 kb of DNA. The small islands of condensed chromatin described in Fig. 8, *A–C*, or the loop of decondensed chromatin visualized in Fig. 8 *F* likely correspond to 50-several hundred kilobases of DNA.

Patterns of Intranuclear DNA Distribution and Chromatin Decondensation Are Characteristic for Specific Times in G1

Inspection of large numbers of survey negatives and smaller

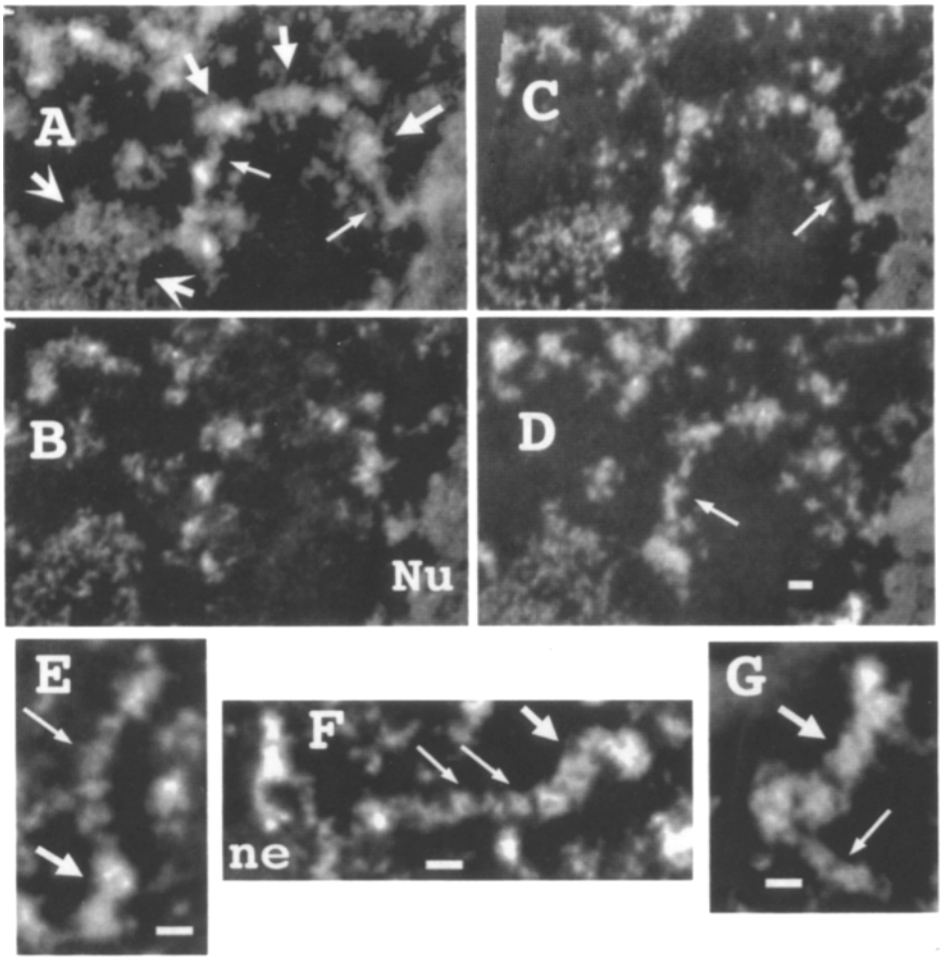

Figure 7. Transitions between different diameter chromonema fibers: (*A–D*) Projection (*A*) through 5, 35-nm thick serial sections and three adjacent serial sections (*B–D*) from a region of a late G1/early S phase nucleus (10 h after release from G1 arrest). Region shows a single chromonema fiber, ~2 μm in length, extended between an apparent attachment site at the edge of a nucleolus (*right*) and the edge of an interchromatin granule cluster (*left*). Thick arrows point to several segments ~120 nm in diameter, separated by segments 60–80 nm in diameter (*thin arrows*). *Nu*, nucleolus. (*E–G*) Show three examples from middle G1 nuclei (2 h after mitosis) again illustrating abrupt transitions of chromonema fibers from 100–130-nm diameter segments (*thick arrows*) to 60–80 nm diameter segments (*thin arrows*). In *F*, 60–80-nm diameter chromonema fiber segment is interrupted by local regions of decondensation suggestive of folding of chromatin fibers (see area between two thin arrows). *ne*, Nuclear envelope. Bars, 120 nm.

numbers of serial section data sets from each time point suggested that patterns of intranuclear DNA distribution and chromatin decondensation were surprisingly characteristic for each sample, with transit through G1 accompanied by progressive chromatid and chromatin decondensation as described above. Interestingly, the pattern of chromatid decondensation and intranuclear distribution after G1 arrest and subsequent release was clearly distinguishable from the sequence of decondensation observed for the G1 cycling synchronization method.

These conclusions were tested more objectively by the following analysis. A single representative nuclear section from each time point was selected; four of the six examples chosen are shown in Figs. 2 and 5. Comparison of these six examples suggested several features that could be used to distinguish each sample. These specific features have already been discussed at great length in the preceding results sections, and they are summarized in Table I.

Between 24 and 30 negatives from each of the six samples were then combined by random shuffling into a single group. Each negative from this group was examined without any identification indicating which sample it was derived from, and was then matched to one of the six representative examples that it most closely resembled. The results are summarized in Fig. 9. At the first time points after mitosis or release from G1 arrest, this classification is particularly accurate with 77% of the G1 cycling 1 h and 92% of the G1 arrest 0 h cells classified exactly; nearly all the remaining cells are matched to the next time point, with <5% of the cells matched to either a late G1 time point or to any time point from the alternative synchronization method. As expected because of loss of cell cycle synchrony during G1, at late time points, the accuracy in classification falls to 50% (G1 cycling) or 70% (G1 arrest); however, essentially all of the remaining nuclei are classified as corresponding to the adjacent time point, or to late G1 nuclei from the alternative synchronization scheme. The accuracy in classifying G1 nuclei from the alternative G1 synchronization methods is also extremely high.

These results demonstrate continuing decondensation of large-scale chromatin packing and changes in the overall intranuclear DNA distribution occurring through the G1 phase, and they confirm the general pattern of G1 chromatid decondensation described above.

Discussion

Summary of Results

Previous work had demonstrated the presence of 100–130-nm large-scale chromatin domains within *Drosophila* and human mitotic chromosomes (Belmont et al., 1989). A satis-

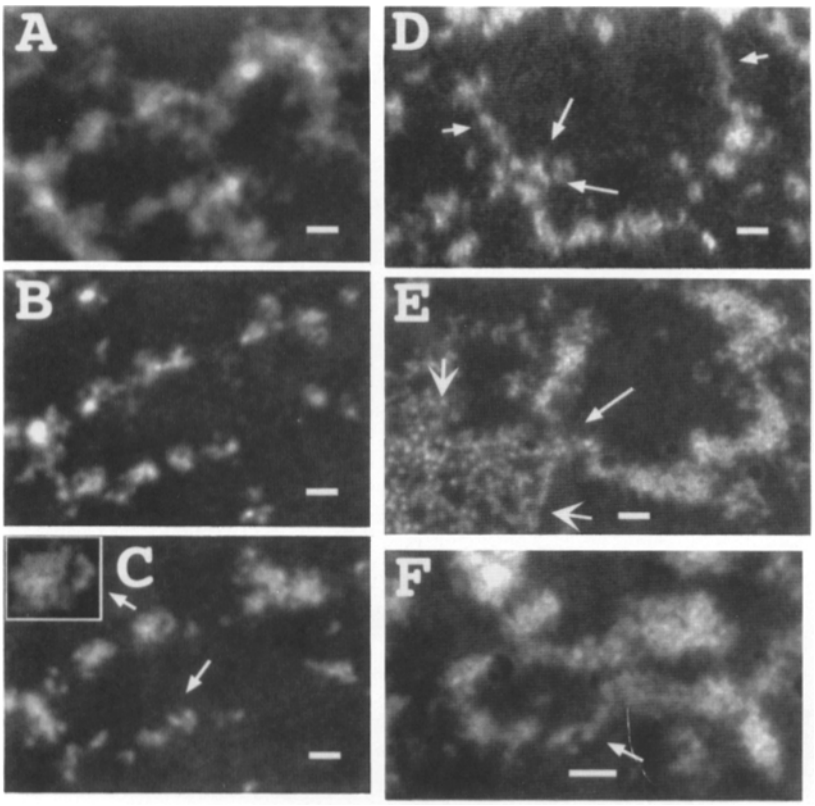

Figure 8. Decondensed regions punctuate chromonema fibers: (*A–C*) An extended chromonema fiber. (*A*) Projection of nine serial sections, 40-nm thick, (*B* and *C*) two adjacent serial sections. Fiber consists of short condensed segments connected by locally decondensed regions; in several of these decondensed regions, folding of 30-nm chromatin fibers is suggested (*lower arrow, C*). (*Inset in C, upper arrow*) 2× enlargement of condensed segment (redigitized at 5.4 nm/pixel) suggestive of substructure consisting of tight folding of higher order chromatin fibers. (*D–F*) Additional examples of local decondensation of chromonema fibers (5.4 nm/pixel digitization). (*D*) Short arrows point to decondensed regions formed by loose folding of extended 20–30-nm fibers. Long arrows point to surrounding diffuse staining material which, speculatively, may represent site of transcription. (*E*) Chromonema fiber shows local decondensation (*thin arrow*) immediately adjacent to interchromatin granule cluster (*curved arrowheads*). (*F*) Loop of decondensed chromatin connecting at separated ends to condensed chromonema fibers. Bars, 120 nm.

factory description of the actual physical structures to which these "domains," visualized in semithick sections, corresponded was not established in this earlier work. In this paper, we have extended this previous work in two significant directions.

First, we have demonstrated unambiguously by serial thin sectioning that in CHO cells, these 100–130-nm large-scale chromatin "domains" in fact correspond to actual fibers. In early G1 nuclei, these 100–130-nm diameter "chromonema" fibers typically can be traced as distinct fibers for lengths of 0.5–1.0 μm, and in selected cases, at later stages in G1 for distances >2 μm. Because in the early G1 nuclei most of the chromatin appears present as 100–130-nm chromonema fibers too tightly coiled to be traced by our serial section reconstructions, it is likely that 0.5–1.0 μm is an underestimate of typical fiber lengths.

In late G1 and early S phase nuclei, more extended and less condensed 60–80-nm large-scale chromatin domains can be traced as distinct chromonema fibers for distances >2 μm. Regions of local unfolding of these chromonema fibers reveal loosely folded and extended 30-nm chromatin fibers, suggesting that these chromonema fibers are formed by the tight folding of 10- and 30-nm chromatin fibers. Chromonema fibers can be visualized looping from the nuclear envelope or nucleolar surface, and extending between the nuclear envelope, nucleoli, or interchromatin granule clusters.

Second, we have described changes in the large-scale chromatin organization during G1 progression with the goal of identifying folding intermediates in the pathway of chromosome decondensation.

In early G1 nuclei, condensed chromatid-like regions were identified, ~0.2–0.4 μm in width, which were concentrated near the nuclear periphery and nucleoli. These likely represent chromosome segments late in decondensation and appear to be formed by the local coiling, with supercoiling and kinking, of 100–130-nm chromonema fibers. Within the same nuclei and at later time points in G1, slightly less condensed chromatin masses were visualized that more clearly demonstrate tight folding of 100–130-nm chromonema fibers into more condensed structures. By examining nuclei later in G1, it was possible to identify condensed regions consisting of isolated kinks or single coils of these chromonema fibers. Overall, our data suggests that the transition from early to middle G1 is accompanied by a progressive uncoiling and extension of these 100–130-nm chromonema fibers; this occurs highly nonsynchronously in different chromosomal regions, and it is accompanied by a dispersal of chromatin to a more uniform distribution within the nuclear interior.

Progression through later stages of G1 and early S phase is associated with further large-scale chromatin decondensation. The trend towards increased dispersal of chromatin throughout the nuclear interior and decreased size and number of chromatid-like condensed masses continues. Also, straightening of chromonema fibers continues, but it is accompanied by a decrease in chromonema fiber diameter. At the later time points for both methods of G1 synchronization, long extended 100–130-nm fibers are infrequently seen. Instead, 100–130-nm fibers are present as shorter segments; more common are extended 60–80-nm chromonema fibers that can be traced as actual distinct fibers within our reconstructions for distances >2 μm. Examples were shown in which an individual 100–130-nm diameter chromonema fiber abruptly changes in diameter to 60–80 nm. Also shown

Table I. Summary of Cell Cycle Differences in Large-scale Chromatin Organization

	G1 cycling (h)			G1 arrest (h)		
Relative frequency	1	2	4	0	4	10
A G1 chromatids	++++	+		++	+	
B Coiled 100–130 nm	++++	++	+	+++	+	
C Extended 100–130 nm	++	+++	+	++	++	+
D Extended 60–80 nm		++	+++	++	+++	+++++
E Peripheral distribution	++++			++++		
F Homogeneous distribution	+	+++	++++		++	+++

Relative frequencies of structures (*A–D*) or extent of agreement with description (*E–F*) are shown for different synchronization time points. Hours represent time after mitosis for G1 cycling, or mitotic shakeoff, synchronization method, and time after release from isoleucine-minus G1 arrest for G1 arrest synchronization method. (*A*) Condensed, linear regions 0.2–0.4 μm in diameter containing 100–130-nm chromonema fibers (see text). (*B*) Regions where 100–130-nm chromonema fibers are kinked and coiled in small condensed aggregates or more loosely coiled within small subvolumes. (*C*) Relatively straight 100–130-nm chromonema fibers. (*D*) Extended 60–80-nm chromonema fibers. (*E*) Concentration of condensed chromatin within 0.5–1.0-μm shell underlying the nuclear envelope. (*F*) Uniformity of chromatin distribution within the nuclear interior.

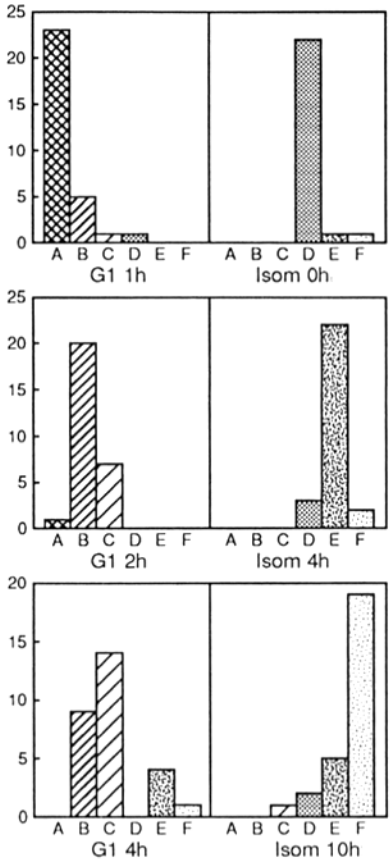

Figure 9. Patterns of decondensation of large-scale chromatin organization are characteristic for different G1 stages. Histograms are shown for classification of randomly selected nuclear cross-sections from different time points. Each negative was matched to one of six nuclei (*A–F*) chosen as representative of a given G1 synchronization sample. Ordinate refers to number of nuclei. *A–C* correspond respectively to nuclei characteristic of 1, 2, and 3.75 h after mitosis in the cycling G1 synchronization procedure. *D–F* correspond, respectively, to nuclei characteristic of 0, 4, and 10 h after release from G1 arrest in the presence of hydroxyurea. (*Left panels*) G1, 1 h (*top*), 2 h (*middle*), and 3.75 h (*G1 4h, bottom*) after mitosis (*Right panels*), 0 h (*top*), 4 h (*middle*), and 10 h (*bottom*) after release from G1 block in the presence of hydroxyurea. Note that not only are the great majority of nuclei correctly matched with the representative nuclei from the corresponding time point, and/or the neighboring time point for later stages of G1, but that there is even better discrimination between nuclei from the two types of G1 synchronization procedure used.

were examples of chromonema fibers that alternated along their length from diameters of 60–80 nm and 100–130 nm. Together, these observations suggest the possibility that the thicker 100–130-nm chromonema fibers may in fact be formed by the helical folding or torsional twisting of 60–80-nm chromonema fibers.

In addition, examples were provided of local decondensation of individual chromonema fibers.

Working Model of Large-scale Chromatin Structure

These observations allow us to propose the following preliminary working model for large-scale chromatin organization, as summarized in Fig. 10. Higher order 30-nm and possibly 10-nm chromatin fibers fold into 60–80-nm chromonema fibers. These 60–80-nm chromonema fibers undergo an additional compaction either through a folding into 100–130-nm chromonema fibers, or possibly through a continuous remodeling process. These larger chromonema fibers, in turn, fold and kink into condensed chromatin masses. A progressive condensation over larger chromosomal regions gives rise to a coalescence of contiguous condensed regions into linear chromatids.

G1 chromatid decondensation is then associated with a progressive unfolding and straightening of 100–130-nm chromonema fibers. This first yields chromonema fibers more loosely coiled than in the condensed chromatids, but still confined to small local subvolumes adjacent to the nuclear envelope and nucleoli, but by later G1 and early S phase produces extended fibers filling the nuclear interior. At the same time, the 100–130-nm chromonema fibers are further decondensing to yield 60–80-nm chromonema fibers.

Note that at all stages of G1 examined, the large-scale chromatin folding patterns are quite heterogenous, indicating a highly nonsynchronous decondensation sequence over different chromosomal regions. In addition, there exist local regions where there is uncoiling of chromonema fibers to individual 30-nm chromatin fibers.

A motivation for our work was to demonstrate unfolding

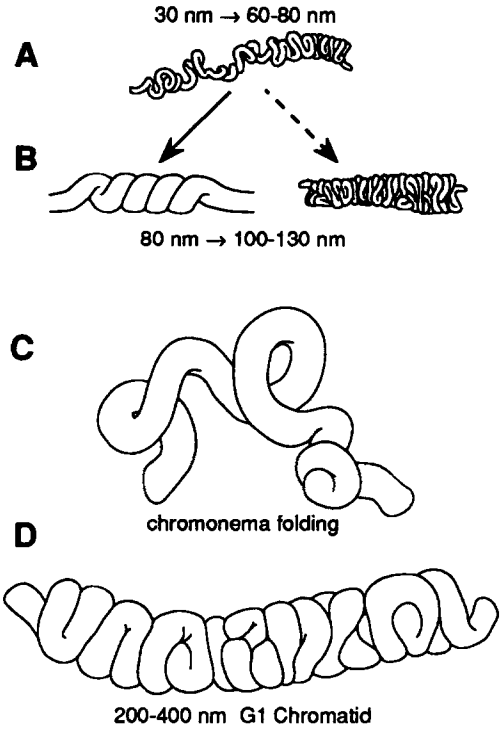

Figure 10. Working model for interphase large-scale chromatin organization. (*A*) Folding of 30-nm higher order chromatin fibers into 60–80-nm chromonema fiber. (*B*) Transition between 60–80-nm chromonema fibers and thicker 100–130-nm chromonema fibers – left side (*solid arrow*) shows a favored model where 60–80 nm fiber coils to form thicker 100–130-nm fiber, right side (*dashed arrow*) shows alternative model where there is a continuous remodeling of the folded 30-nm chromatin fibers to form a thicker chromonema fiber. (*C*) Folding, twisting, supercoiling of chromonema fibers leads to small condensed masses separated by more extended fibers. (*D*) Irregular folding of 100–130-nm chromonema fibers into condensed G1 chromatids (see text), 0.2–0.4 μm in diameter. Drawings were sketched from clay models.

intermediates of large-scale chromatin organization; we expect that there is a continuous and sequential pathway for chromosome decondensation/condensation such that intermediates identified in early G1 or late G2 nuclei are themselves found folded and compacted within more condensed mitotic chromosomes. The model we present, however, is based on observations from G1 nuclei where chromatids condensed over the entire chromosome length are not present.

Therefore, the suggestion in our model that mitotic chromatids are formed by the folding and kinking of the 100–130-nm chromonema fibers is based on a synthesis of our results for G1 nuclei with additional published and unpublished works. Specifically, previously published work (Belmont et al., 1990) suggested 100–130-nm large-scale chromatin "domains" within mitotic and telophase chromosomes from *Drosophila* and human somatic cells. These regions, suggestive of packing of actual fibers 100–130 nm in diameter, are more clearly demonstrated in buffers containing higher concentrations of polyamines or divalent cations. EM tomographic reconstructions (Belmont, A. S., J. W. Sedat, and D. A. Agard, unpublished data) also showed more clearly these 100–130-nm fiberlike regions within metaphase and anaphase chromosomes; however, because of the tight packing within the chromosome, these regions were separated by only 10–30 nm, and it was not possible to demonstrate unambiguously that these domains were produced by actual spatially distinct fibers. Finally, in addition to the analysis of large-scale chromatin decondensation during G1 described in this paper, we have also examined large-scale chromatin condensation during G2 and early prophase using similar methodology. Our results to date (Li, G. L., K. Bruce, and A. S. Belmont, manuscript in preparation) are consistent with the model presented above, including the transitions between 60–80-nm chromonema fibers to 100–130-nm chromonema fibers and the folding of 100–130-nm chromonema fibers within 0.2–0.3-μm prophase chromatids.

In Vivo vs In Vitro Large-scale Chromatin Structure

A very important question obviously is how the large-scale chromatin structure that we describe in our work relates to the actual in vivo structure. This larger question can be broken into several more specific questions: (*a*) What conformational changes are induced during detergent permeabilization in the polyamine buffer? (*b*) What changes may be induced by glutaraldehyde fixation? (*c*) What changes are induced by alcohol dehydration and embedding?

Several different lines of experimental observations suggest that conventional dehydration and embedding protocols do not significantly alter large-scale chromatin organization at the level of structure focused on in this paper. Comparison of chromatin preservation in sperm nuclei after conventional Epon embedding, low temperature embedding in the hydrophilic resin Lowicryl K-11, freeze substitution, and freezing in vitreous ice followed by frozen sectioning revealed improved preservation of the internal structure of the 30-nm chromatin fiber using low temperature methods but no change in the intranuclear packing of 30-nm chromatin fibers (Horowitz et al., 1990; Woodcock, 1994). More specifically, the diameter decreased during conventional embedding; however, the characteristic arrangement of 30-nm fibers within these echinoderm nuclei after Epon embedding was identical to that observed in frozen sections (Woodcock, 1994). Low temperature embedding of HeLa nuclei, permeabilized and fixed according to the same methods used in this paper for CHO nuclei, revealed no apparent change in large-scale chromatin organization relative to conventional Epon embedding (unpublished data). Finally, preliminary experiments using atomic force microscopy to examine the surface topology of mitotic chromosomes isolated in buffer A are revealing surface features consistent with the large-scale chromatin chromonema fibers described in this paper (Yang, G., G. Li, A. S. Belmont, and C. Bustamante, unpublished data).

The same studies of echinoderm sperm nuclei cited above also demonstrated no change in the internal structure of the 30-nm chromatin fiber or its arrangement within nuclei after glutaraldehyde fixation; in fact, glutaraldehyde fixation before freeze substitution appeared to improve the consistency of structural preservation.

Therefore, we believe the most critical step in our specimen preparation procedure is the first: extraction with detergent and exposure of nuclei to a particular isolation buffer.

As reported in a previous paper, quite dramatic changes in large-scale chromatin structure as a function of chromosome isolation buffer conditions, particularly divalent and polycation concentrations, were demonstrated by light microscopy (Belmont et al., 1989); for instance, low concentrations of polycations led to mitotic chromosomes without the sharp boundaries visualized in living cells, as well as the loss of fine internal structure within interphase nuclei. However, observations within living cells (Belmont et al., 1989) and cells fixed in glutaraldehyde without previous detergent extraction, as described in Fig. 1, are suggestive of a fibrous large-scale chromatin organization consistent with the chromonema fiber organization. Also, no apparent change in this large-scale chromatin organization is observed when cells are detergent permeabilized in the polyamine buffer A before fixation.

Furthermore, in our previous study, we showed by EM (Belmont et al., 1989) that the widths of large-scale chromatin domains were quite similar between telophase nuclei from cells fixed with or without previous detergent permeabilization. Likewise, numerous previous publications show micrographs of metaphase and interphase chromosomes within unpermeabilized cells fixed in physiological buffers with features indicative of the large-scale chromonema fibers we describe (Setterfield et al., 1978; Adolph, 1980; Alberts et al., 1989; Benavente et al., 1989; Garcia-Segura et al., 1989). This includes a recent study using both freeze substitution and DNA-specific staining techniques (Bohrmann and Kellenberger, 1994).

Together, these previous works therefore argue strongly that the large-scale chromonema fibers described in this paper reflect actual large-scale chromatin fibrous structures existing in living cells.

Relationship to Previous Work

The most significant conclusion from our work is the existence of at least one and possibly two distinct higher order "chromonema" fibers above the 30-nm chromatin fiber within interphase nuclei. These results are incompatible with previous radial loop models of chromosome structure. However, our observations are not incompatible with the actual published data from which such models were derived. This data consists largely of two sets of observations. First are observations from histone-depleted, mitotic chromosomes where apparent loops of DNA are visualized emanating from a residual protein scaffolding (Paulson and Laemmli, 1977). This data is problematic in two respects. Because of the harsh treatments, it is difficult to separate cross-linking occurring in vitro from that preexisting in vivo. Much more serious is the size of the residual "protein scaffolding," comparable to that of the native chromosome, and the extremely high packing ratios found in both mitotic and interphase chromosomes. What appears as a closed loop when decondensed as naked DNA and viewed at low magnification may be appreciated as a quite different topology after compaction into higher order chromatin structures.

The second set of observations are based on partially swollen mitotic chromosomes, in which 30-nm chromatin fibers, approximately radially oriented, are seen protruding from a dense central region through which fibers could not be traced (Marsden and Laemmli, 1979; Adolph, 1980). Again, however, the size of this dense central region is large relative to the diameter of the original native chromosome, and it is not possible to trace the 30-nm fibers within this central region to determine directly whether these fibers were present as actual loops. In fact, tomographic reconstructions of similarly swollen chromosomes in which 30-nm fibers have been traced over substantial distances have failed to observe any radial loop organization (Harauz et al., 1987).

Nearly all previous work addressed at large-scale chromatin folding patterns existing above the level of the 30-nm chromatin fiber has focused on the structure of mitotic chromosomes. As discussed in the introduction section, this has led to serious experimental limitations arising from the high packing density and complexity of mitotic chromosome structure. By focusing on the unfolding of G1 chromatids, we have bypassed many of these experimental problems and allowed visualization of levels of chromatin folding above the 30-nm chromatin fiber by using simple serial thin sectioning approaches. Moreover, unlike previous models based on observations of metaphase chromosomes, our focus on unfolding intermediates has led naturally to an integrated model of mitotic and interphase chromatid structure.

Finally, we note that the predicted DNA packing ratios implied by a folded chromonema model of mitotic chromosome structure, discussed below, are consistent with recent in situ hybridization results showing a separation across the width of a metaphase chromatid of probes 1 Mbp apart (Lawrence et al., 1990). Moreover, a folded chromonema model of interphase chromatid structure is consistent with preliminary in situ localization of amplified dihydrofolate reductase genes in a chromosomal homogeneously staining region using a new technique with improved ultrastructural preservation. Lac repressor staining is used to visualize the location of dihydrofolate reductase genes marked by multiple lac operator copies. Optical sectioning light microscopy and electron microscopy show extended fiber paths within interphase nuclei (Robinett, C. C., C. W. Willhelm, G. L. Li, and A. S. Belmont, manuscript in preparation).

Biological Implications

Assuming a DNA linear packing ratio of 37:1 for the 30-nm chromatin fiber, just one loop or zig-zag of a 30-nm fiber across and back the width of a 130-nm chromonema fiber would correspond to 28 kb of DNA. These long chromonema fibers, on the order of 0.5–2.5 μm in length, therefore consist of very large DNA stretches. A rough minimum estimate formed by calculating the packing ratio for a two-dimensional zig-zag pattern of 30-nm loops across the width of the fiber yields 28 kb/60 nm of fiber length or ~470 kb/μm chromonema fiber length, a packing ratio of 160:1. The actual packing ratio for the 130-nm chromonema fiber is likely to be several-fold larger because of the three dimensional nature of its structure. Similarly, the packing ratio for the 60–80-nm chromonema fibers is expected to be several-fold lower but still considerable. Thus, a rough estimate of the compaction range of these chromonema fibers would be 160–1,000:1, consistent with the range estimated by in situ hybridization for probes separated by several hundred kilobases within interphase nuclei (Lawrence et al., 1990).

Experimentally, increased DNase 1 sensitivity has been used to demonstrate the existence of large chromatin domains, in some cases, hundreds of kilobases in size, sur-

rounding transcriptionally competent loci (Eissenberg et al., 1985). It is tempting to speculate that local decondensation of chromonema fibers, as illustrated in Fig. 8, may correspond to such chromatin domains.

Folding of 10- and 30-nm chromatin fibers within these chromonema fibers might still be organized through "scaffolding" proteins whose self assembly drives this large-scale chromatin folding. In this respect, it is of interest that nuclear scaffolding preparations appear to contain fiberlike features of similar size to the chromonema fibers described in this paper (Hozak et al., 1993). Alternatively, chromatin fibers could be anchored through nonspecific interfiber interactions at multiple sites distributed over extended regions, and not necessarily restricted to the base of actual chromatin loops. These interactions may in fact lead to self-folding of chromatin fibers modulated by various histone modifications and by specific nonhistone proteins, such as heterochromatin-binding proteins. Nonhistone proteins could contribute either by modulating the folding of individual chromatin fibers, by stabilization of chromonema fibers, or even higher level compaction of chromonema fibers, through interfiber crosslinking interactions.

Independent of the mechanisms involved, the folded chromonema model of largescale chromatin folding would not require that *cis*-acting sequences controlling chromatin domain structure correspond to actual bases of closed chromatin loops. Extended or looped 10- and 30-nm chromatin fibers could be anchored at their ends through interactions with condensed chromatin within adjacent chromonema fibers. This would lead to open loops or even extended fibers, as observed recently for Balbiani Ring active chromatin in polytene chromosomes (Ericsson et al., 1989). Moreover, the spacing between such control regions could be much more complex than predicted by a radial loop model.

Finally, a folded chromonema model of large-scale chromatin organization lends itself easily to cooperative interactions extending over very large DNA lengths. Such interactions over very large DNA regions may be involved, for instance, in developmental gene complexes such as Bithorax and *Antennapedia* in *Drosophila*. The synchronous firing of multiple replicon units, distributed over regions hundreds of kilobases to megabases in length, may also involve cooperativity in large-scale chromatin folding over comparable distances.

We thank Rick Olson for expert technical assistance and development of procedures for thin-section serial sectioning. We thank David Agard and John Sedat for providing mechanical drawings, for duplicating their optical sectioning light microscope system, and for early distribution of the data collection program "Resolve3D". We also thank Mel Jones, Hans Chen, and John Minden for technical assistance during the assembly and testing of the microscope system. Transmission electron microscopy was carried out at the Center for Electron Microscopy at the University of Illinois, Champaign-Urbana.

This work was supported by National Institutes of Health grant R29 GM-42516, NSF grant DIR-8907921, and a Whitaker Foundation grant to Andrew Belmont.

Received for publication 8 June 1994 and in revised form 28 July 1994.

References

Adolph, K. W. 1980. Organization of chromosomes in mitotic HeLa cells. *Exp. Cell Res.* 125:95–103.

Agard, D. A., Y. Hiraoka, P. Shaw, and J. W. Sedat. 1989. Fluorescence microscopy in three dimensions. *Methods Cell Biol.* 30:353–377.

Alberts, B., D. Bray, J. Lewis, M. Raff, K. Roberts, and J. D. Watson. 1989. Molecular Biology of the Cell. Garland Publishing, Inc., New York. 1218 pp.

Belmont, A. S., M. B. Braunfeld, J. W. Sedat, and D. A. Agard. 1989. Large-scale chromatin structural domains within mitotic and interphase chromosomes in vivo and in vitro. *Chromosoma (Berl.).* 98:129–143.

Belmont, A. S., J. W. Sedat, and D. A. Agard. 1987. A three-dimensional approach to mitotic chromosome structure: evidence for a complex hierarchical organization. *J. Cell Biol.* 105:77–92.

Belmont, A. S., Y. Zhai, and A. Thilenius. 1993. Lamin B distribution and association with peripheral chromatin revealed by optical sectioning and electron microscopy tomography. *J. Cell Biol.* 123:1671–1685.

Benavente, R., M. C. Dabauvalla, U. Scheer, and N. Chaly. 1989. Functional role of newly formed pore complexes in postmitotic nuclear reorganization. *Chromosoma (Berl.).* 98:233–241.

Bjorkroth, B., C. Ericsson, M. M. Lamb, and B. Daneholt. 1988. Structure of the chromatin axis during transcription. *Chromosoma (Berl.).* 96: 333–340.

Bohrmann, B., and E. Kellenberger. 1994. Immunostaining of DNA in electron microscopy: an amplification and staining procedure for thin sections as alternative to gold labeling. *J. Histochem. Cytochem.* 42:635–643.

Boy de la Tour, E., and U. K. Laemmli. 1988. The metaphase scaffold is helically folded: sister chromatids have predominately opposite helical handedness. *Cell.* 55:937–944.

Burke, B., and L. Gerace. 1986. A cell free system to study reassembly of the nuclear envelope at the end of mitosis. *Cell.* 44:639–652.

Eissenberg, J. C., I. L. Cartwright, G. H. Thomas, and S. C. R. Elgin. 1985. Selected topics in chromatin structure. *Annu. Rev. Genet.* 19:485–536.

Enger, M. D., R. A. Tobey, and A. G. Saponara. 1968. RNA synthesis in Chinese hamster cells. I. Differential synthetic rate for ribosomal RNA in early and late interphase. *J. Cell Biol.* 36:583–593.

Ericsson, C., H. Mehlin, B. Bjorkroth, M. M. Lamb, and B. Daneholt. 1989. The ultrastructure of upstream and downstream regions of an active Balbiani Ring gene. *Cell.* 56:631–639.

Garcia-Segura, L. M., M. Lafarga, M. T. Berciano, P. Hernandez, and M. A. Andres. 1989. Distribution of nuclear pores and chromatin organization in neurons and glial cells of the rat cerebellar cortex. *J. Comp. Neurol.* 290:440–450.

Harauz, G., L. Borland, G. F. Bahr, E. Zeitler, and M. van Heel. 1987. Three-dimensional reconstruction of a human metaphase chromosome from electron micrographs. *Chromosoma (Berl.).* 95:366–374.

Heck, M. M. S., and W. C. Earnshaw. 1986. Topoisomerase 2: a specific marker for cell proliferation. *J. Cell Biol.* 103:2569–2581.

Hiraoka, Y., J. R. Swedlow, M. R. Paddy, D. A. Agard, and J. W. Sedat. 1991. Three-dimensional multiple-wavelength fluorescence microscopy for the structural analysis of biological phenomena. *Semin. Cell Biol.* 2:153–165.

Hodge, L. D., J. E. Martinez, W. C. Allsbrook, C. G. Pantazis, and D. A. Welter. 1990. Intermediate structures in nuclear morphogenesis following metaphase from HelaS3 cells can be isolated and temporally grouped. *Chromosoma (Berl.).* 99:169–182.

Horowitz, R. A., P. J. Giannasca, and C. L. Woodcock. 1990. Ultrastructural preservation of nuclei and chromatin: improvement with low-temperature methods. *J. Microsc.* 157:205–224.

Hozak, P., A. B. Hassan, D. A. Jackson, and P. R. Cook. 1993. Visualization of replication factories attached to a nucleoskeleton. *Cell.* 73:361–373.

Lafond, R. E., and C. L. F. Woodcock. 1983. Status of the nuclear matrix in mature and embryonic chick erythrocyte nuclei. *Exp. Cell Res.* 147:31–39.

Lawrence, J. B., R. H. Singer, and J. A. McNeil. 1990. Interphase and metaphase resolution of different distances within the human dystrophin gene. *Science (Wash. DC).* 249:928–932.

Lloyd, D., R. K. Poole, and S. W. Edwards. 1982. The Cell Division Cycle. Academic Press, London. 523 pp.

Marsden, M. P. F., and U. K. Laemmli. 1979. Metaphase chromosome structure: evidence for a radial loop model. *Cell.* 17:849–858.

Paulson, J. R., and U. K. Laemmli. 1977. The structure of histone depleted chromosomes. *Cell.* 12:817–828.

Rattner, J. B., and C. C. Lin. 1985. Radial loops and helical coils coexist in metaphase chromosomes. *Cell.* 42:291–296.

Sedat, J., and L. Manuelidis. 1977. A direct approach to the structure of eukaryotic chromosomes. *Cold Spring Harbor Symp. Quant. Biol.* 42:331–350.

Setterfield, G., R. Sheinin, I. Dardick, G. Kiss, and M. Dubsky. 1978. Structure of interphase nuclei in relation to the cell cycle. *J. Cell Biol.* 77:246–263.

Spector, D. L. 1993. Macromolecular domains within the cell nucleus. *Annu. Rev. Cell Biol.* 9:265–315.

Tobey, R. A., and H. A. Crissman. 1972. Preparation of large quantities of synchronized mammalian cells in late G1 in the pre-DNA replicative phase of the cell cycle. *Exp. Cell Res.* 75:460–464.

Tobey, R. A., and K. D. Ley. 1970. Regulation of initiation of DNA synthesis in Chinese hamster cells. I. Production of stable, reversible G1-arrested populations in suspension culture. *J. Cell Biol.* 46:151–157.

Welter, D. A., D. A. Black, and L. D. Hodge. 1985. Nuclear reformation following metaphase in HelaS3 cells. Three-dimensional visualization of chromatid rearrangements. *Chromosoma (Berl.).* 93:57–69.

Woodcock, C. L. 1994. Chromatin fibers observed in situ in frozen hydrated sections. Native fiber diameter is not correlated with nucleosome repeat length. *J. Cell Biol.* 125:11–19.

Xing, Y. G., C. V. Johnson, P. R. Dobner, and J. B. Lawrence. 1993. Higher level organization of individual gene transcription and RNA splicing. *Science (Wash. DC).* 259:1326–1330.